Materials Advances

ROYAL SOCIETY OF CHEMISTRY

PAPER

View Article Online
View Journal | View Issue

Cite this: *Mater. Adv.*, 2024, 5, 5644

Long-lasting anti-swelling sustained-release estradiol hydrogel for promoting vaginal wound healing

Tianyue Zhang,[ab] Hongyi Lv,[c] Yijing Zhang,[ab] Lingyun Yu,[d] Yonghong Li,[d] Hechun Yan,[ab] Chenyan He,[e] Dongmei Zhao,[a] Lijuan Zhao,[c] Yuedong He,*[a] Yi Wang *[c] and Zhongyi Zhu *[ab]

In both clinical and research settings, the rapid healing of vaginal injuries remains a significant challenge globally. Conventional treatment methods often involve extended recovery periods and increased risk of retrograde infections, causing significant pain and discomfort for patients. To address this issue, a mechanically robust and stable poly(hydroxyethyl methacrylate) (PHEMA)/alginate hydrogel loaded with estrogen has been developed to facilitate vaginal wound repair. This hydrogel is formed by an ionically crosslinked alginate network and a covalently crosslinked PHEMA network, which effectively enhances network strength and dissipates energy, leading to excellent fatigue resistance and anti-swelling behavior. Its exceptional mechanical stability and anti-swelling properties prevent local adhesions and mucosal ischemic necrosis. Additionally, the hydrogel sustains the release of estradiol, promoting vaginal epithelial proliferation and collagen deposition, thereby significantly accelerating vaginal injury healing. Furthermore, the hydrogel eliminates the need for frequent dressing changes, reducing the risk of retrograde infections. The hydrogel demonstrates outstanding biocompatibility both *in vitro* and *in vivo*. These combined advantages enable the hydrogel to reduce vaginal recovery time, prevent adhesions, and lower the risk of infection. Therefore, the estrogen-loaded PHEMA/alginate hydrogel demonstrates great potential for achieving satisfactory healing in cases of vaginal injury.

Received 20th February 2024,
Accepted 29th May 2024

DOI: 10.1039/d4ma00173g

rsc.li/materials-advances

1 Introduction

Vaginal injuries in women are quite common, with the primary causes including childbirth,[1] surgery,[2] sexual activity,[3] and trauma by accidents,[4] which may lead to varying degrees of damage to the vaginal mucosa, muscles, or other tissues. Vaginal delivery is one of the most common causes of vaginal injuries, where tearing, cutting, and stretching during childbirth can cause severe vaginal trauma. Certain vaginal surgeries, such as vaginal reconstruction required for patients with Mayer–Rokitansky–Küster–Hauser (MRKH) syndrome, also result in extensive vaginal injuries.[5] After vaginal reconstruction surgery, the most common problem is that tissue fibrosis leads to vaginal stenosis,[6] even to lifelong scar sequelae or the need for reoperation,[7] so vaginal dilatation is the most common requirement after surgery.[8] Vaginal molds are often used in clinic to achieve the effect of vaginal dilatation, and patients need to wear hard vaginal molds for a long time. Long-term mold compression will lead to tissue ischemia, hypoxia, cell deformation and death, and then cause tissue necrosis.[9,10] Some growth factors, such as exosomes, have been proven experiments to promote the healing of vaginal wounds *in vitro*[11] and *in vivo*.[12] However, the extraction process of exosomes is complex, and their storage conditions are stringent, making it impractical for widespread clinical use. Therefore, there is an urgent need for the development of new materials that can promote growth and act as an alternative to silicone molds in preventing adhesion.

Estrogen is a type of steroid hormone, encompassing various components such as estrone, estradiol, and estriol. Estrogen cream is commonly used for atrophic vaginitis, is cost-effective, and easily accessible. Currently, the role of estrogen in

[a] *Department of Gynecology and Obstetrics, West China Second University Hospital, Sichuan University, Chengdu, 610041, China. E-mail: heyuedong@scu.edu.cn, zhuzhongyi92@139.com*
[b] *Key Laboratory of Birth Defects and Related Diseases of Women and Children, West China Second University Hospital, Sichuan University, Ministry of Education, Chengdu, 610041, China*
[c] *College of Chemistry and Materials Science, Key Laboratory of the Evaluation and Monitoring of Southwest Land Resources (Ministry of Education), Sichuan Normal University, Chengdu, 610068, China. E-mail: wangyi2020@sicnu.edu.dn*
[d] *The People's Hospital of Wenjaing Chengdu, Chengdu, 611130, China*
[e] *Sichuan Normal University, Chengdu, 610068, China*

promoting vaginal growth has been substantiated by numerous studies. Ovariectomy in rabbits, followed by the local application of estrogen to the vagina, has been shown to enhance vaginal wound healing and improve biomechanical recovery.[13] In ovariectomized rats, the use of estrogen in the vagina increases the thickness of the vaginal epithelium and upregulates gene expression related to epithelial barrier function and protease inhibition.[14] Local estrogen treatment enhances the content of total and cross-linked collagen, and significantly stimulates the expression of collagen mRNA.[15] At the molecular level, estrogen is involved in the regulation of various genes, including those known to regulate cell growth and proliferation, barrier function, and defense against pathogens, within several key pathways, such as Erk/Akt pathway.[16] As a supplementary medication, local estrogen application fosters the growth of vaginal epithelium. In contrast to systemic estrogen administration, localized estrogen usage has a limited impact on circulating estrogen levels[17,18] and does not significantly elevate the risk of cardiovascular disease or cancer.[19] At present, local vaginal administration of estrogen is often achieved through estrogen creams or suppositories, requiring daily application to the vaginal wound, which can be inconvenient for patients and increase the risk of retrograde infections. Therefore, there is a lack of materials that can provide sustained release of estrogen while also offering support and fixation for the treatment of vaginal defects.

Hydrogels, as a novel biomedical three-dimensional porous material, are considered to be the most promising option to achieve sustained release of drug at specific disease locations.[20–24] The hydrogel for post-vaginal injury needs the following characteristics. Firstly, it needs a certain hardness to act as a physical barrier, replacing molds, and prevent vaginal adhesions that lead to narrowing. Secondly, it should exhibit long-term resistance to swelling because post-vaginal injury, there is often a significant amount of local exudate. If the hydrogel absorbs water and expands, it could compress vaginal tissues, leading to necrosis. The robust and tightly woven interpenetrating cross-linked network imparts the hydrogel with outstanding anti-swelling properties. Kim *et al.* developed a highly tough, non-swelling hydrogel by integrating covalent and ionic cross-linked networks.[25] Thirdly, the hydrogel will remain in the patient's vagina for an extended period, subject to repeated bending and folding due to patient movements, necessitating good mechanical properties and fatigue resistance. Currently, many studies are focused on optimizing the mechanical properties of hydrogels through various approaches. Ma *et al.* prepared a double-network hydrogel with dynamic borate ester bonds and hydrogen bonds, which was shown to possess high mechanical strength and toughness. Yang *et al.* enhanced the mechanical properties of hydrogels by implementing multiple hydrogen bond interactions.[26] Zhang *et al.* prepared ionically and chemically cross-linked double-network hydrogels with high tensile strength and elastic modulus based on sodium alginate and a kind of antifouling material, *N*-hydroxyethyl acrylamide (HEAA).[27] Sun *et al.* synthesized highly stretchable and tough hydrogels by combining ionically cross-linked alginate and covalently cross-linked polyacrylamide. The integration of weak and strong cross-links significantly increased the fracture energy of the hydrogels, allowing these hydrogels, which contain 90% water, to stretch over 20 times their original length.[28] Li *et al.* fabricated alginate-polyacrylamide hydrogels combining short-chain and long-chain alginates to reduce the viscosity of the pre-gel solution and synthesized homogeneous hydrogels with high ionic cross-linking density to enhance mechanical properties.[29] Gorke *et al.* optimized the mechanical properties of calcium alginate/polyacrylamide double-network hydrogels by varying four parameters: the concentration of alginate (c_{Alg}), the mixing ratio of high/low molecular weight alginate (R_p), the concentration of acrylamide (c_{AAm}), and the concentration of *N*,*N*′-methylenebisacrylamide (c_{MBA}).[30] Fourth, hydrogels need to have good biocompatibility. Kim *et al.* used biocompatible PHEMA and alginate as raw materials to fabricate hydrogels with excellent biocompatibility, achieving 99% cell viability over 60 days.[25] The alginate/polyacrylamide interpenetrating network gels fabricated by Darnell *et al.* can maintain high viability of murine mesenchymal stem cells.[31] Lastly, the recovery process from severe vaginal injury is prolonged, and incorporating growth factors into the hydrogel could shorten this process. In recent years, hydrogels with controllable biological activity have been widely used for treating internal wounds.[32–34] They encapsulate estrogen,[35] cytokines,[36] cells, or exosomes,[37] forming a delivery system to release therapeutic components for the treatment of internal wounds.

Herein, a mechanically robust and stable poly(hydroxyethyl methacrylate) (PHEMA)/alginate (SA) hydrogel loaded with estradiol (E2) by mesoporous silica (SiO_2) is designed to act as a suitable platform to promote vaginal wound repair. As shown in Scheme 1, this hydrogel uses poly(hydroxyethyl methacrylate) (PHEMA) as the base for its good biocompatibility. *N*,*N*′-Methylenebisacrylamide (MBA) is incorporated to establish chemical crosslinks. Additionally, sodium alginate (SA) and Ca^{2+} are added to form dynamic ionic coordination crosslinks between carboxyl groups and Ca^{2+}. Additionally, estradiol-loaded silica nanoparticles (E2@SiO_2) are embedded, ensuring their uniform distribution within the physical–chemical hybrid crosslinking network of the hydrogel.

The hybrid network and ionic crosslinking-induced phase separation jointly contribute to improved network strength and effective energy dissipation, imparting excellent mechanical properties, fatigue resistance and anti-swelling property to the hydrogel. Even after 14 days of swelling, the hydrogel still maintains its excellent mechanical properties, making it an effective support material for vaginal defect treatment. Experiments on vaginal defects in rats demonstrate that this hydrogel significantly promotes wound growth and reduces healing time. This kind of drug loaded hydrogel with good biocompatibility, fatigue resistance, anti-swelling and controllable drug release is expected to be used as an ''estrogen-fixed support combination'' to achieve the treatment of vaginal wounds, and this work provides a new idea for the treatment of vaginal defects.

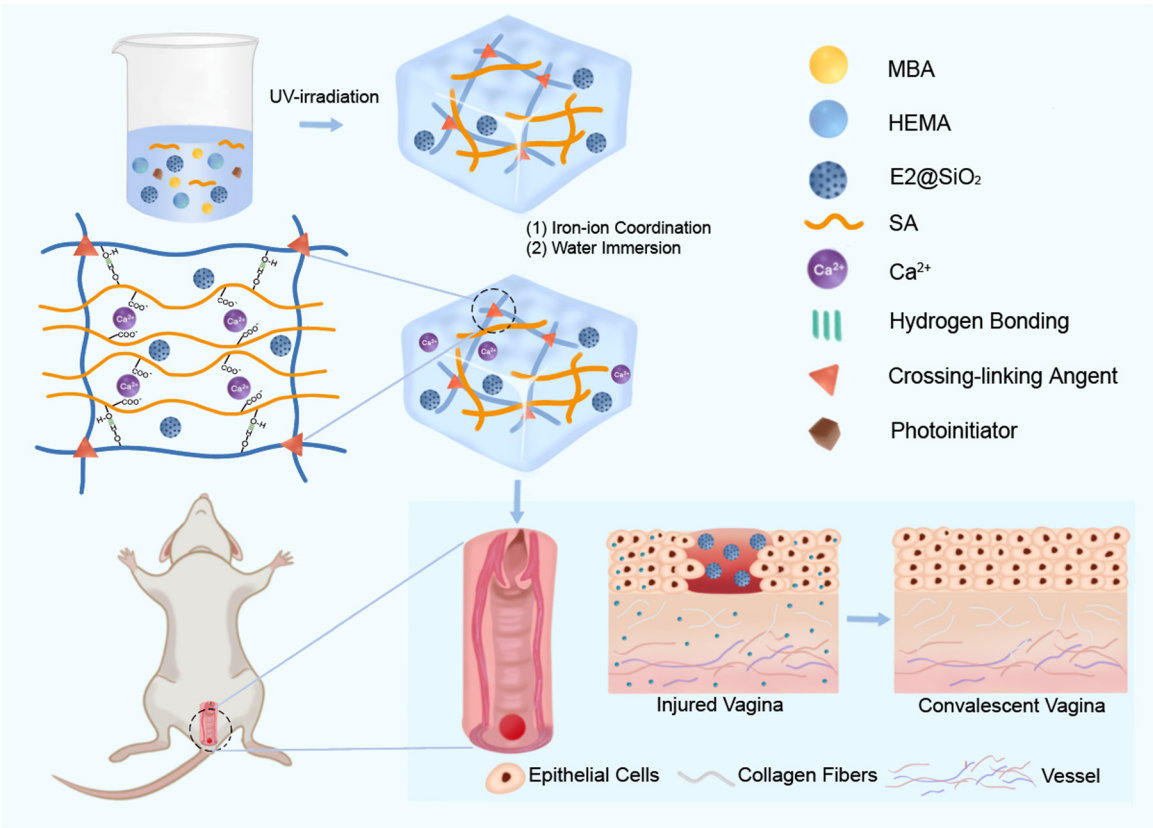

Scheme 1 This figure illustrates the raw materials, preparation process, and the application of PSH hydrogel in the treatment of wounds.

2 Experimental section

2.1 Materials

2-Hydroxyethyl methacrylate (HEMA), *N*,*N*′-methylenebisacrylamide (MBA), and hexadecyl trimethyl ammonium bromide (CTAB) were provided by Adamas, China. Sodium alginate (SA), tetraethyl orthosilicate (TEOS), sodium hydroxide (NaOH), concentrated hydrochloric acid (HCl), and anhydrous ethanol were provided by Chengdu Kelong Chemical Reagent Factory, China. Calcium chloride dihydrate ($CaCl_2{\cdot}2H_2O$) and estradiol (E2) were provided by Shanghai Aladdin Biochemical Technology, China. The photoinitiator 2-hydroxy-2-methylacetone (Irgacure1173) was provided by TCI (Shanghai) Chemical Industry Development Co., Ltd. Deionized water was self-made by Sichuan Normal University.

2.2 Preparation of drug loaded nano silica microspheres (E2@SiO_2)[35]

Firstly, 1 g CTAB, 480 mL water, 96 mL anhydrous ethanol, and 4 mL 1 mol L^{-1} NaOH solution were sonicated and uniformly dispersed in a 1000 mL three necked flask. Then, the solution was heated to 70 °C under magnetic stirring. After CTAB was completely dissolved, 6 mL of TEOS was added to the three necked flask at a rate of 0.1 mol L^{-1} min^{-1}, and the reaction continued for 3 hours under condensation reflux. The product obtained from the reaction was centrifuged and cleaned with water and anhydrous ethanol, and vacuum dried it at 60 °C for 12 hours. The washed product was placed in a vacuum at 60 °C for 12 hours to remove moisture and other volatile substances. CTAB is a commonly used template agent in the synthesis of mesoporous silica, forming an ordered structure that generates mesoporous structures during the polymerization of the silane precursor. After product formation, CTAB needs to be removed to expose the mesoporous structure. A mixed solvent of 37 wt% hydrochloric acid-ethanol was used for extraction to remove the template agent CTAB from the product. During the extraction step, the dried product was placed in the hydrochloric acid-ethanol solution and stirred thoroughly to ensure full contact between CTAB and the solvent, allowing it to be extracted. The extracted solution was then centrifuged to separate the solid and liquid phases. The solid part after centrifugation is the mesoporous silica with the template agent removed. The solid part was washed with an appropriate amount of deionized water and ethanol to remove residual hydrochloric acid and CTAB. Multiple washes ensure thorough removal of the template agent. The washed solid product was dried again to obtain pure mesoporous silica nanoparticles. Finally, 0.5 g of SiO_2 was uniformly dispersed in 20 mL of estradiol ethanol solution (50 mg mL^{-1}) and stirred for 24 hours in a closed conical flask. After centrifuging, cleaning, and drying, silica nanospheres loaded with estradiol (E2@SiO_2) were obtained. In our previous research, we fabricated silica (SiO_2) with a mesoporous spherical structure. Through Brunauer–Emmett–Teller (BET) testing, we determined that these materials have an average pore

size of 3.3 nm and a surface area of 1009.5 $m^2 g^{-1}$. Such structural properties are highly advantageous for drug carriers.[35]

2.3 Preparation of anti-swelling drug loaded PHS hydrogel

At room temperature, 10 g of HEMA, 0.5 g of SA, 20 mg of MBA, and 20 mg of E2@SiO_2 were dissolved in 30 g of deionized water. After stirring the mixture evenly, the solution was placed under a nitrogen atmosphere for deoxygenation for 30 minutes. Subsequently, 50 μL of Irgacure1173 was added and gently stirred until uniform. The solution was then poured into a mold and irradiated under a 250 W UV lamp for 30 minutes to 1 hour to cure and form the polymer. The cured polymer block was removed from the mold, cut into appropriate sizes, and soaked in a 2 mol L^{-1} $CaCl_2$ solution, allowing it to stand at room temperature for 24 hours to enable the coordination of Ca^{2+} with the carboxyl groups in the hydrogel. The coordinated hydrogel blocks were then taken out of the $CaCl_2$ solution and washed repeatedly with deionized water to remove residual $CaCl_2$. Finally, the hydrogel blocks were soaked in deionized water for 24 hours for swelling treatment. The resulting hydrogel was named PHS hydrogel.

The polymer was prepared from the same amount of HEMA and MBA under the same conditions, and then soaked in water for 24 hours, named PHM hydrogel.

2.4 Structural characterization

Scanning electron microscope (SEM): PHS hydrogel was frozen in the refrigerator, and then put into a freeze dryer to freeze dry for 48 hours. EV018 SEM was used to observe the cross-section morphology of the freeze-dried sample, and the working voltage was 20 kV during the test.

Fourier transform infrared spectrometer (FTIR): after freeze-drying PHM and PHS hydrogel samples, Nicolet Magna IR560 FTIR was used to test, and the test wavelength is 400–4000 cm^{-1}.

Small angle X-ray scattering (SAXS): the SAXS experiment was conducted at room temperature at the Shanghai Synchrotron Radiation Facility (SSRF), using an X-ray wavelength of 0.124 nm. Software Foxtrot was used to perform background correction and processing on SAXS patterns for further analysis.

2.5 Rheological measurements

Variable temperature frequency scanning test: the rheological properties of PHM and PHS hydrogels were characterized by TA AR2000ex rheometer. The sample were prepared in circular flakes (diameter: 40 mm, thickness: 2 mm). The frequency scanning tests were carried out on the hydrogel. The temperature range was 20 °C to 65 °C, the frequency range was 1–100 rad s^{-1}, and the strain was 0.05%. Based on the principle of time-temperature equivalence, the storage modulus G', loss modulus G'', and loss factor $\tan\delta$ at different temperatures were calculated. The main curves of the rheological wide frequency range were obtained by shifting and stacking the curves, with 20 °C as the reference temperature. The horizontal displacement factor α_T of time temperature superposition conforms to the Arrhenius equation:[38]

$$\alpha_T = e^{-E_a/RT} \quad (1)$$

After taking the logarithm of both sides, the equation is transformed into:

$$\ln \alpha_T = -E_a/RT \quad (2)$$

Where E_a is the apparent activation energy, R is the gas constant, and T is the testing temperature.

Frequency scanning test: MCR 302 rheometer was used to conduct frequency scanning test on PHM and PHS hydrogels. The samples were prepared into round sheets (diameter: 25 mm, thickness: 2 mm). The test was conducted at a fixed strain of 0.1% and a frequency of 0.1–100 rad s^{-1}.

Strain scanning test: MCR 302 rheometer was used to carry out strain scanning test on PHM and PHS hydrogels. The samples were prepared into round sheets (diameter: 25 mm, thickness: 2 mm). The test was carried out at a constant frequency of 10 rad s^{-1} and a strain of 0.1–100%.

2.6 Mechanical properties measurements

The tensile and fatigue properties of hydrogels were systematically tested at room temperature using Instron 3367 universal tensile testing machine (1 kN sensor). In the tensile test, the dumbbell shaped specimens were stretched at a speed of 100 mm min^{-1} until fracture, and the corresponding tensile stress–strain curves were recorded on the computer software. In order to evaluate the fatigue resistance of hydrogels, cyclic loading–unloading compression tests with strain of 20% and 50% were carried out at the speed of 100 mm min^{-1}.

2.7 Swelling performance test

Using the quality analysis method, the PHS hydrogel samples were cut with the same size, and recording the weight as W_0. The hydrogel specimens were put into phosphate-buffered saline (PBS) for swelling, and the hydrogel samples were weighed every other period of time, and recording it as W_d. The swelling ratio SR is determined by the following formula. Each sample was tested three times and the average value was taken to ensure the validity of the swelling test results.

$$SR = \frac{W_d - W_0}{W_0} \times 100\% \quad (3)$$

2.8 E2 release experiment

The hydrogel was cut into square pieces with sides measuring 2 cm and placed in centrifuge tubes containing 10 mL of PBS. The centrifuge tubes were stored at a constant temperature of 37 °C for 30 days. Samples of 300 μL were collected daily for ten consecutive days to determine the concentration of E2, and an equal volume of PBS was added to the centrifuge tubes to maintain the total liquid volume. The concentration of estradiol in the samples was measured using an estradiol ELISA assay kit.

2.9 *In vitro* biocompatibility experiment

Human vaginal epithelial cells VK2/E6E7 (CRL-2616) were purchased from the American Type Culture Collection and cultured in keratinocyte-serum free medium (GIBCO, USA).

The preparation of hydrogel extract followed established methods, with the hydrogel soaked in the cell culture medium at a concentration of 0.1 g ml^{-1} for 24 hours. The medium containing the hydrogel extract was filtered through a 0.22 μm filter to remove bacteria. Human vaginal epithelial cells were seeded in 96-well plates at a density of 4000 cells per well. After 24 hours, the original culture medium was replaced with normal culture medium and hydrogel extract, serving as the control and experimental groups, respectively. After 1, 3, and 5 days of culture, the cells were stained using the Calcein-AM/PI dual staining reagent (Solarbio, China), where live cells appeared green, and dead cells appeared red under an inverted fluorescence microscope. ImageJ was used for quantitative analysis. Following the above protocol, the cells were also seeded in 24-well plates at a density of 10 000 cells per well. After 24 hours, the original culture medium was replaced with normal culture medium and hydrogel extract, serving as the control and experimental groups, respectively. The IncuCyte S3 Live-Cell Analysis System (Sartorius, USA) was used to monitor cell confluence, with images taken every 8 hours over a period of 120 hours.

2.10 *In vivo* biocompatibility experiment

PHS hydrogel was implanted into the dorsal region of rats. After 14 days, the dorsal tissue containing the hydrogel was retrieved, fixed with formaldehyde (Solarbio, China), embedded in paraffin, and then subjected to HE staining and IL-6 immunohistochemical staining.

2.11 Establishment and treatment of rat vaginal defect model

All animal procedures in this study were approved by the Institutional Animal Care and Use Committee of West China Second University Hospital, Sichuan University (Approval No: WCSUH21-2023-037). Sprague-Dawley rats (180–220 g, 6–8 weeks old) were purchased from Sichuan Dashuo and housed in the Experimental Animal Center of West China Second Hospital, Sichuan University. 15 rats, isolated for one month, were randomly divided into three groups: control group, mold group, and hydrogel group, with 5 rats in each group. After anesthetizing the rats using an isoflurane inhalation anesthesia system, the fur around the vaginal orifice was removed, and the vaginal orifice was sterilized. A standardized vaginal defect model was created by making a perforation at the distal end of the rat's vagina using a 3 mm skin punch. Subsequently, in the mold group, a silicone mold was inserted into the rat's vagina, and in the hydrogel group, PHS hydrogel was placed in the rat's vagina. The control group rats received no treatment. The vaginal condition of the rats was observed and photographed daily for 1–5 days after surgery. On the 5th day, the PHS hydrogel was removed from the rat's vagina. Vaginal tissues were collected and fixed with formaldehyde for subsequent experiments. ImageJ software was used for quantitative assessment of wound area.

2.12 Histological analysis

Rat vaginal tissues were paraffin-embedded, sectioned, and subjected to H&E staining, Masson's staining, and Ki-67 immunohistochemical staining, followed by whole-slide scanning. The percentage of fibrosis area and the analysis of cell numbers were both performed using ImageJ software. The evaluation of staining results was conducted using the IHC score, which assigned 3 points for strongly positive areas, 2 points for positive areas, 1 point for low positive areas, and 0 points for negative areas. The quantification of IHC scores was facilitated by the IHC Profiler plug-in within the ImageJ software.

2.13 Statistical analysis

All data were obtained from at least three repeated tests. Two-group comparisons were analyzed using the *t*-test, while comparisons involving three or more groups were analyzed using analysis of variance (ANOVA). All data are reported as mean ± standard deviation. Significance levels are indicated as follows: * $p < 0.05$, ** $p < 0.01$, *** $p < 0.001$, and **** $p < 0.0001$, representing statistically significant differences.

3 Results and discussion

3.1 Design and characterization of PHS hydrogel

A mechanically robust and stable PHEMA/SA hydrogel loaded with E2@SiO_2 is designed as a support material for the treatment of vaginal defects. The hydrogel is prepared by the polymerization of HEMA with the introduction of SA, MBA and E2@SiO_2, and then soaked in $CaCl_2$ solution and deionized water to form ionic crosslinking interactions. As a result, a hybrid network composed of chemical cross-linking and ionic cross-linking is successfully constructed. The chemical cross-linking helps maintain network elasticity while the ionic cross-linking induces significant phase separation to effectively dissipate energy. Therefore, the hydrogel possesses excellent mechanical properties, fatigue resistance, anti-swelling properties and sustained drug releasing ability. These unique properties not only enable the hydrogel to act as a fixed material to support the vaginal structure, but also facilitate long-term and slow release of E2, thereby promoting the proliferation and regeneration of vaginal epithelial cells to achieve the vaginal wounds healing. The resulting hydrogel is named as PHS hydrogel. For comparison, a hydrogel without SA and Ca^{2+} is fabricated in the same way and named as PHM hydrogel.

The structure of the PHS hydrogel is characterized by scanning electron microscope (SEM), Fourier transform infrared spectrometer (FTIR), small angle X-ray scattering (SAXS) and rheological tests. As shown in Fig. 1A, a dense and stable three-dimensional network structure is formed in the PHS hydrogel, which enables the PHS hydrogel to be placed in the vagina as an effective support material, and is conducive to the stable release of E2. In addition to the network structure, the network interaction is also analyzed. Compared to the FTIR spectra of the PHS hydrogel, the characteristic peak of O–H in the PHS hydrogel moves from 3527.7 cm^{-1} to 3442.8 cm^{-1} (Fig. 1B), indicating that the hydrogen bond interaction in PHS hydrogel is stronger than that in PHM hydrogel. This can be attributed to the introduction of SA, which enhances the hydrogen bonds in the network of the PHS hydrogel. Stronger hydrogen bond

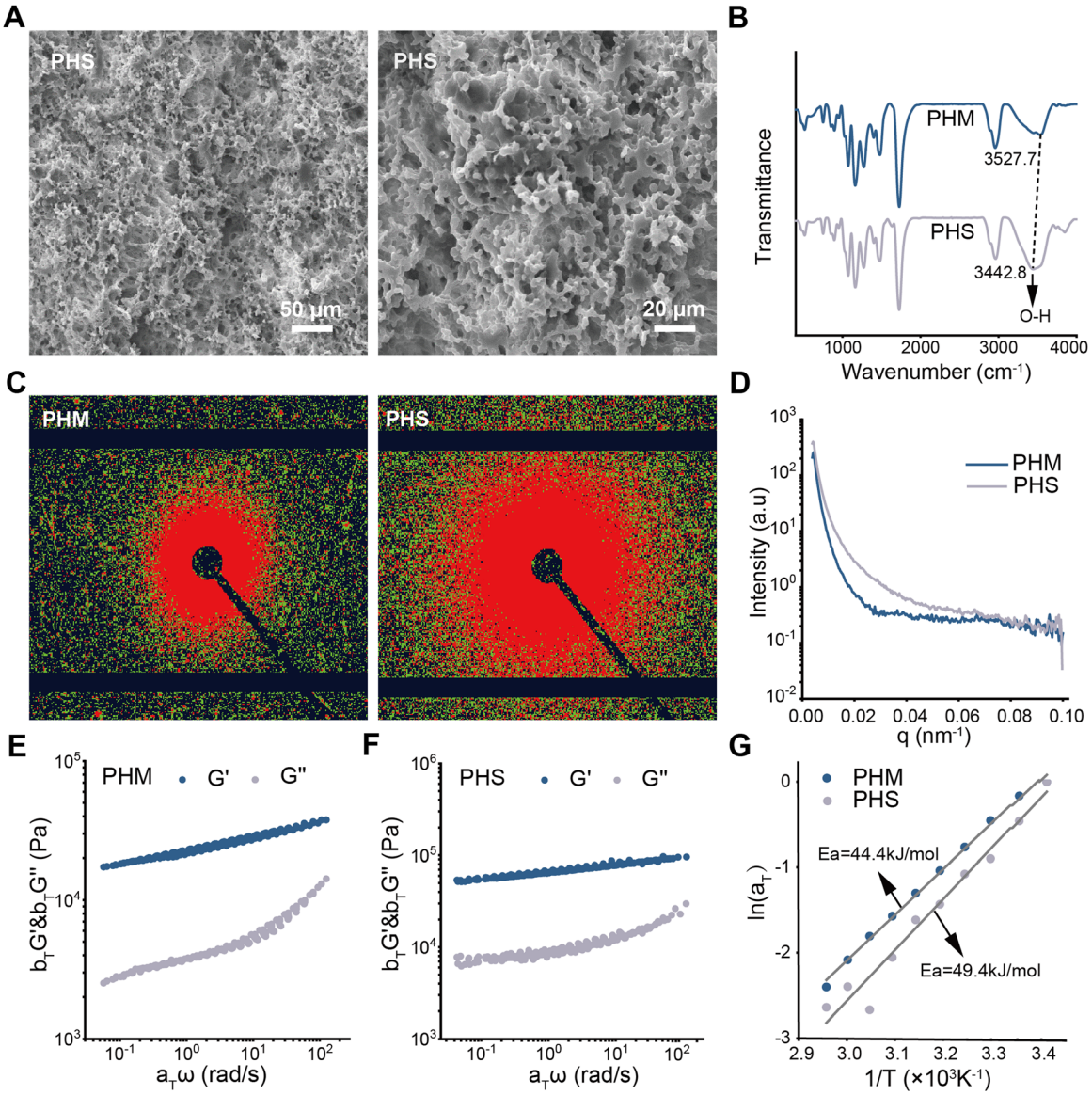

Fig. 1 Structural and internal interaction characterization of the hydrogels. (A) SEM images of the PHS hydrogel. (B) Infrared absorption spectra of the PHM hydrogel and PHS hydrogel. (C) 2D SAXS diagram of the PHM hydrogel and PHS hydrogel. (D) ID strength distribution diagram corresponding to the PHM hydrogel and PHS hydrogel. (E) and (F) Master curves of frequency dependence of G' and G'' of the PHS hydrogel by time-temperature superposition shifts at reference temperature of 20 °C. (G) Representative Arrhenius plots for the temperature dependent shift factors a_T, where the apparent activation energy E_a is determined by the slope of the linear fitted lines.

interactions make the internal network of the PHS hydrogel more compact, improving its mechanical performance.

Notably, the introduction of the ionic cross-linking between SA and Ca^{2+} promotes phase separation in the PHS hydrogel, proved by SAXS. In the SAXS 2D images, the larger the radius of the circles, the more pronounced the phase separation in the hydrogel network, indicating a less uniform network distribution.[39] As shown in the SAXS 2D diagram, the PHM hydrogel exhibits phase separation to some extent because of the aggregation and entanglement of PHEMA chains in the hydrogel network (Fig. 1C), forming a heterogeneous structure of phase separation. After introducing the ionic cross-linking interactions, the scattering signal and scattering intensity of the PHS hydrogel are further enhanced (Fig. 1C and D), implying that the ionic cross-linking interactions intensify the aggregation and entanglement of PHEMA chains, leading to more evident phase separation. Heterogeneous phase separation can form a multiphase structure, where the hard phase provides strength and rigidity, and the soft phase provides flexibility and elasticity. Such a composite structure can significantly enhance the mechanical properties of the hydrogel.[40] PHS hydrogels provide a physical barrier with sufficient strength and hardness while also offering flexibility and elasticity to accommodate the user's daily activities.

The network interaction is further characterized by the rheological measurements. The frequency sweep tests of the

PHM and PHS hydrogels are carried out at 20–65 °C. At different temperatures, the storage modulus G' and loss modulus G'' vary with frequency and then undergo translation and superposition. The main curves are obtained by following the principle of time-temperature superposition (Fig. 1E and F). The relationship between the temperature and the horizontal displacement factors α_T of the hydrogels is shown in Fig. 1G. According to Arrhenius equation, the apparent activation energy E_aa of the PHM hydrogel is 44.4 kJ mol^{-1} while the apparent activation energy E_a of PHS hydrogel increases to 49.4 kJ mol^{-1}, indicating that the PHS hydrogel network becomes more compact and stronger after the introduction of ion coordination interaction. The above results demonstrate a hybrid network with distinct phase separation is successfully constructed in the PHS hydrogel, which is beneficial for the hydrogel to support the vagina and provide a sustained releasing platform during the healing process.[41,42]

3.2 Mechanical properties and anti-swelling properties of the PHS hydrogel

The unique network endows the PHS hydrogel with excellent mechanical and anti-swelling properties. Although the tensile breaking strain of the PHS hydrogel is slightly lower than that of the PHM hydrogel, the tensile modulus, toughness and tensile strength of the PHS hydrogel are far higher than those of the PHM hydrogel (Fig. 2A and B). This shows that with the enhancement of hydrogen bond interactions and the

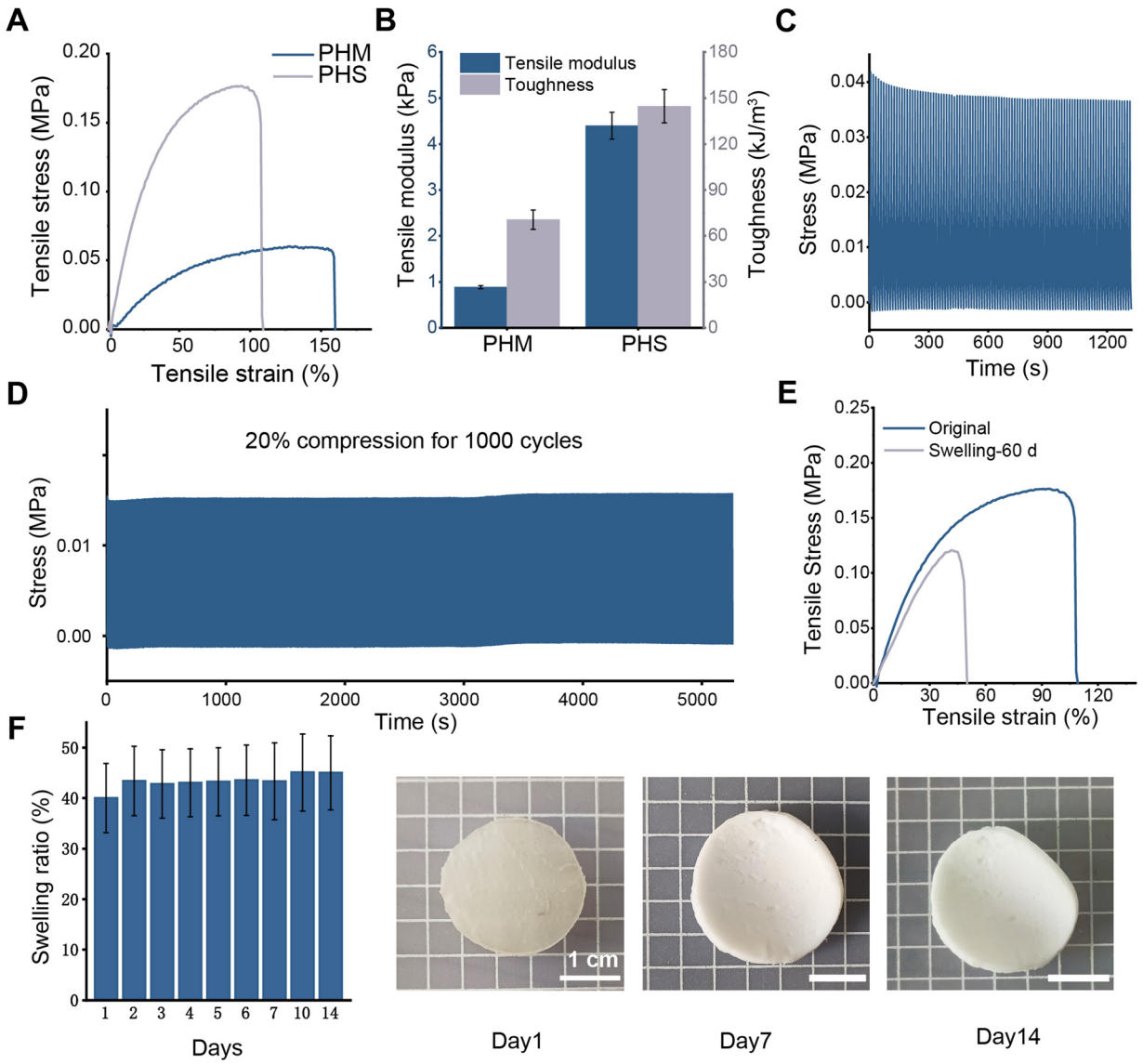

Fig. 2 Mechanical properties and swelling properties of the hydrogels. (A) and (B) Tensile stress–strain curves of PHM hydrogel and PHS hydrogel and their corresponding tensile modulus and toughness histograms. (C) PHS hydrogel is subjected to 100 consecutive compression loading unloading curves at the maximum strain of 50%. (D) PHS hydrogel is subjected to 1000 consecutive loading unloading compression curves at the maximum strain of 20%. (E) Tensile stress–strain curve of PHM hydrogel before swelling and 14 days after swelling. (F) The swelling ratio of PHS hydrogel after 14 days and the physical pictures after 1, 7 and 14 days of swelling.

introduction of ion coordination interactions significantly improve the mechanical properties.

Besides, the PHS hydrogel possesses outstanding fatigue resistance. For different application scenarios, 1000 times loading–unloading cyclic compression tests on PHS hydrogel under low strain (20%) and 100 times loading–unloading cyclic compression tests under high strain (50%) at a high speed of 100 mm min^{-1} are conducted (Fig. 2C and D). The results shows that the compression strength of the PHS hydrogel is almost unchanged under the loading–unloading compression test of 1000 times of continuous compression. Meanwhile, the compression strength of the PHS hydrogel is only decreased by 5.29 kPa after 100 times of loading–unloading compression tests under 50% high strain, showing excellent fatigue resistance and mechanical stability.

Moreover, tough and compact hybrid cross-linking network imparts great anti-swelling performance to the PHS hydrogel as well. To explore the feasibility of the PHS hydrogel in the treatment of vaginal defects, the PHS hydrogel is immersed into PBS for 14 days. Normally, the vaginal environment is acidic, but vaginal injuries can lead to a change in pH. The wound site exudes interstitial fluid with a pH of approximately 7.40,[43] altering the vagina's natural acidic environment to a neutral one. A PBS buffer with a pH of 7.4 is used to simulate the neutral environment of an injured vagina. As shown in Fig. 2F, the swelling ratio of the PHS hydrogel maintains at a relatively stable level. The swelling ratio of the PHS hydrogel is 43.33% after 7 days of swelling, while the swelling ratio of the hydrogel sample is only 45.03% after 14 days of swelling, which is only 3.32% and 5.02% higher than that at the first day. During this process, the shape of the PHS hydrogel samples remain stable and the size is almost unchanged. Furthermore, the break strain remains 48.17% of the original level and the tensile strength remains 68.37% of the original level after 60 days of swelling in water (Fig. 2E). The above results indicate that the PHS hydrogel has long-term and excellent anti-swelling performance, ensuring the hydrogel can be placed in the vagina for a long time as a support and fixation material. Based on the above properties, the PHS hydrogel is expected to be used as a support and fixation material for the treatment of vaginal defects.

3.3 E2-releasing capability

E2, the most potent form of estrogen, has been demonstrated in various studies to promote the growth of vaginal epithelial cells.[44] Therefore, E2 was selected to be loaded onto drug carrier nano silica microspheres (E2@SiO_2) and evenly distributed within the PHS hydrogel. PHS hydrogel requires extended placement in the wound site, serving as both a drug carrier and a mechanical barrier. Its ability to stably and continuously release the drug (E2) over an extended period is crucial for promoting wound healing. To validate the E2 release capability of PHS hydrogel, it was placed in PBS, and the E2 release from PHS hydrogel over ten days was measured. Fig. 3A and B display the total amount of E2 released and the daily release rate of E2, respectively, over ten days. E2 exhibited the highest release on the first day, followed by a daily decrease until it reached a steady state on the fifth day, with an average daily release of 74.77 ng ml^{-1}. The ability of PHS hydrogel to consistently release E2 demonstrates its suitability for long-term vaginal treatment. This sustained release relies on the uniform pore structure within PHS hydrogel and the hydrophobic interactions and hydrogen bonding between E2 and SiO_2 microspheres.

In cases of extensive vaginal injuries, complete wound healing can take several months or even longer due to the slow growth of vaginal epithelium. PHS hydrogel possesses excellent mechanical stability and resistance to swelling, allowing it to remain in the wound site for extended periods. It serves as a mechanical barrier to prevent vaginal adhesions while continually releasing E2. This sustained release ensures a localized E2 concentration at the wound site, mitigating potential systemic side effects associated with systemic hormone use.

3.4 Biocompatibility experiment

Outstanding biocompatibility is a critical characteristic that hydrogels intended for long-term vaginal wound treatment

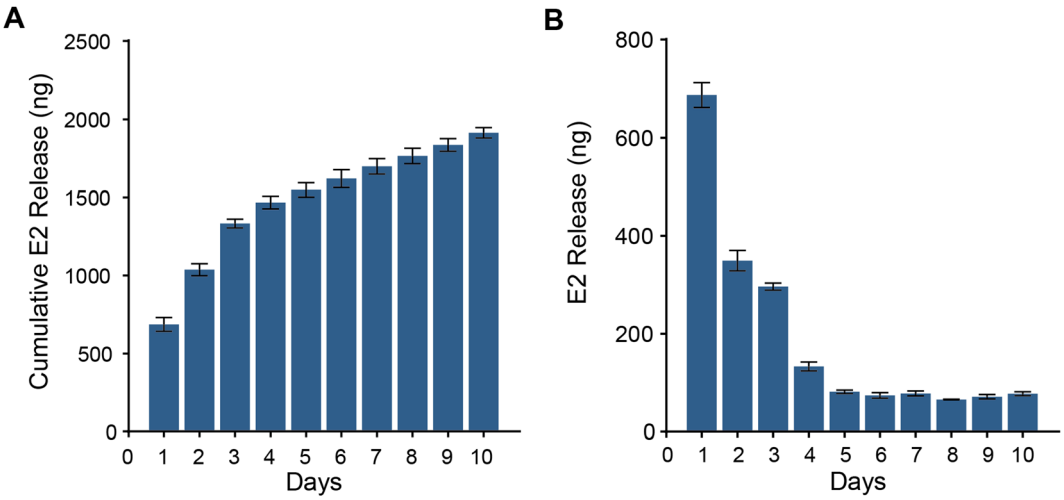

Fig. 3 PHS hydrogel sustained release of E2 over ten days. (A) Cumulative release of E2 over ten days. (B) Daily release of E2 over the ten-day period.

must possess. To evaluate the biocompatibility of PHS hydrogel, we employed various methods. In an elution model, live/dead cell staining, cell counting kit-8 (CCK-8) cell viability assay, and real-time cell imaging using the Incucyte S3 system were employed to assess the cytotoxicity of PHS hydrogel on VK2 vaginal epithelial cells. Fig. 4A displays the results of live/dead cell fluorescence staining for the control group and the PHS hydrogel group, where all VK2 cells in both groups appeared green (indicating live cells) and exhibited normal morphology, with hardly any red cells (indicating dead cells)

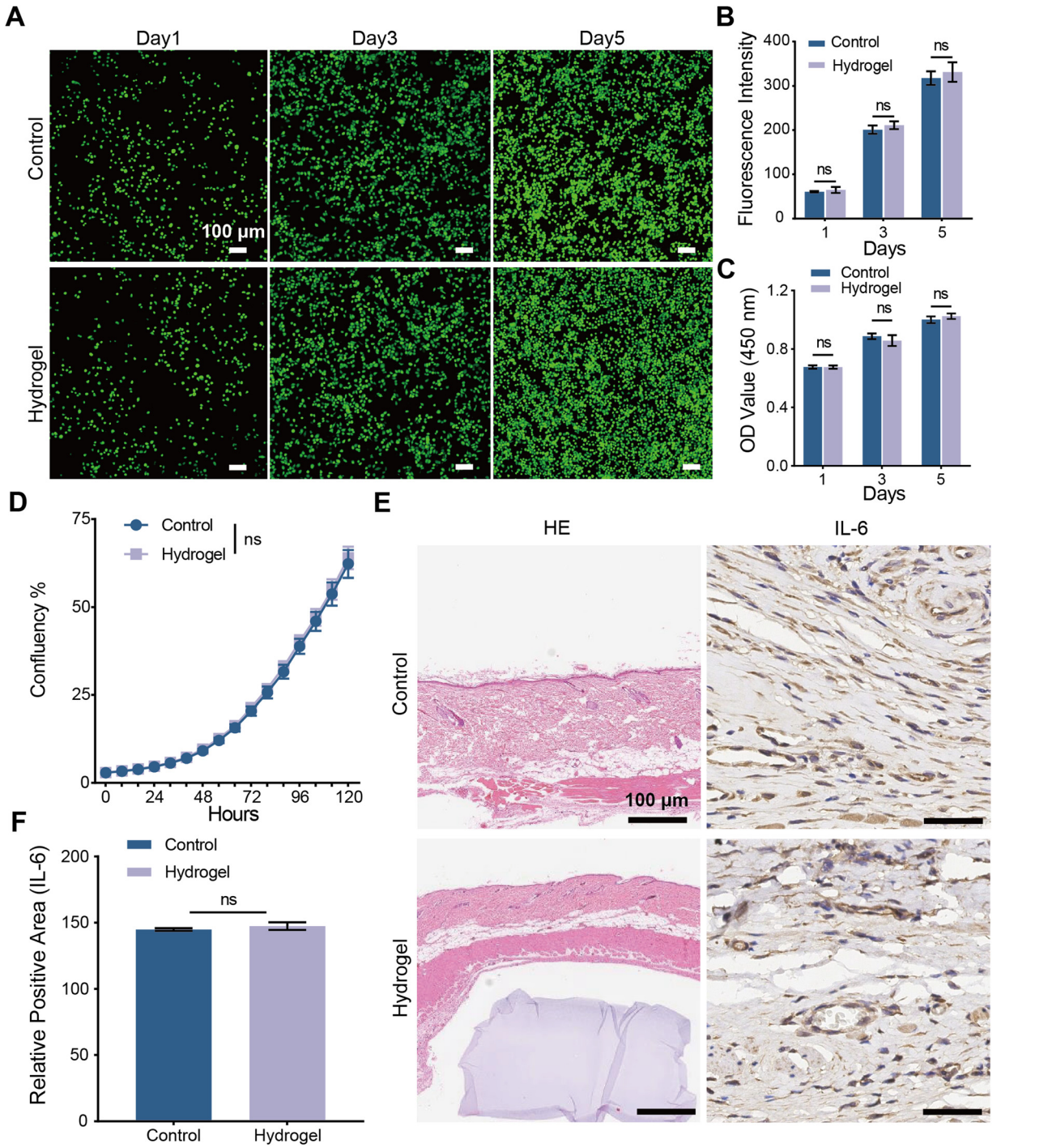

Fig. 4 *In vitro* and *in vivo* compatibility experiments of the hydrogel. (A) Fluorescence images of live/dead staining of cells from the control group and hydrogel group at days 1, 3, and 5. (B) Corresponding area of live/dead cell fluorescence staining. (C) Assessment of cell viability in the control group and hydrogel group at days 1, 3, and 5 using CCK-8. (D) Evaluation of cell proliferation in the control group and hydrogel group using IncuCyte S3 from days 1 to 5. (E) HE and IL-6 immunohistochemical staining of rat dorsal skin with hydrogel implants for 2 weeks. (F) Statistical analysis of the IL-6 immunohistochemical staining positive areas. All data are reported as mean ± standard deviation. NS represents no significant difference.

observed. Quantitative analysis using ImageJ revealed that the relative fluorescence density in the PHS hydrogel group and the control group continued to increase on days 1, 3, and 5, with no statistically significant differences (Fig. 4B). Fig. 4C presents the results of the CCK-8 assay, showing that the cell viability of VK2 cells in both groups exhibited no significant differences on days 1, 3, and 5. Fig. 4D illustrates real-time cell imaging conducted over 120 hours, with images captured every 8 hours, demonstrating similar cell confluence in VK2 cells between the two groups.

To further investigate the *in vivo* biocompatibility of PHS hydrogel, we implanted the hydrogel into the dorsal skin of rats, and after 14 days, we collected samples for hematoxylin and eosin (HE) staining as well as interleukin-6 (IL-6) immunohistochemical staining. As shown in Fig. 4E, the morphology of the dorsal skin with implanted PHS hydrogel appeared normal compared to the dorsal skin of normal rats in the HE staining, indicating that PHS hydrogel can be placed in the body for an extended period without causing fusion with surrounding tissues or inflammation. IL-6 is a critical cytokine that promotes inflammation in tissue damage. Immunohistochemical staining for IL-6 and quantitative analysis of the positive areas (Fig. 4F) showed no significant differences between the two groups, confirming that PHS hydrogel does not induce inflammation when placed in the body.

In the design and fabrication of PHS hydrogel, HEMA[45] and SA,[46] which have been demonstrated to exhibit excellent biocompatibility, were utilized as raw materials to ensure the biocompatibility and safety of PHS hydrogel. The various *in vitro* and *in vivo* biocompatibility tests conducted above have confirmed that PHS hydrogel possesses outstanding cell safety and biocompatibility. This suggests that PHS hydrogel can be

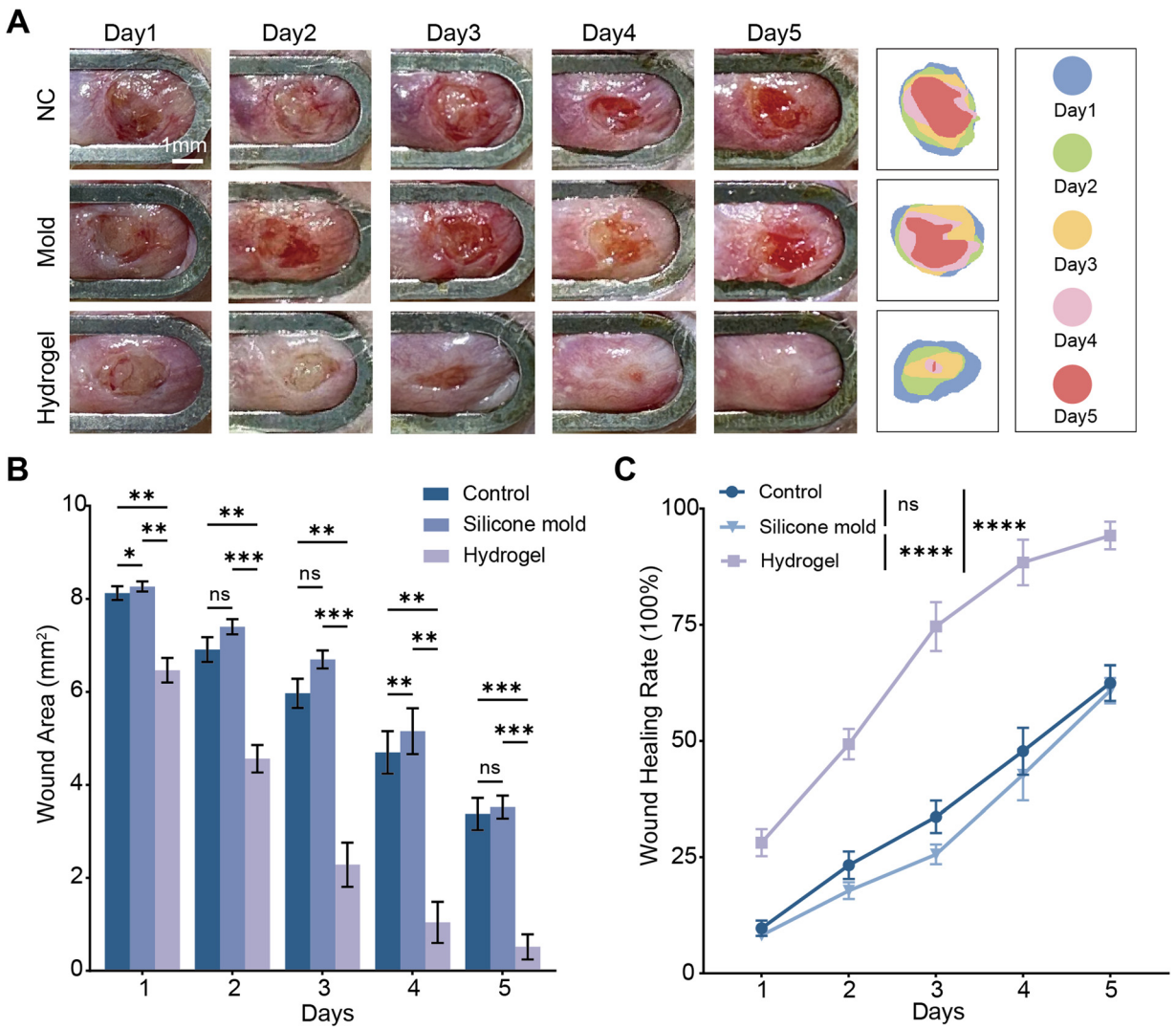

Fig. 5 The therapeutic effect of PHS hydrogel on vaginal wounds in rats. (A) Vaginal wound healing in rats from the NC group, mold group, and PHS hydrogel group on postoperative days 1–5 (measured using a 2.85 mm caliber probe). (B) Quantitative analysis of wound area on days 1–5. (C) Wound healing scores on days 1–5. All data are reported as mean ± standard deviation. Significance levels are indicated as follows: * $p < 0.05$, ** $p < 0.01$, *** $p < 0.001$, and **** $p < 0.0001$. NS represents no significant difference.

employed as a drug delivery system and mechanical support for wound treatment.

3.5 *In vivo* wound healing

The above experimental results demonstrate that PHS hydrogel exhibits excellent mechanical properties, has the capability for sustained release of E2 as a drug delivery system, and possesses outstanding biocompatibility. This suggests that PHS hydrogel holds promise as an ideal material for repairing vaginal wounds. To evaluate the wound healing effect of PHS hydrogel, we established a standardized rat vaginal defect model with three groups, each consisting of 5 rats: (1) control group, receiving no treatment to promote wound healing; (2) mold group, where sterile silicone molds were inserted into the vaginal cavity of model rats, simulating the clinical use of silicone molds in vaginal reconstruction surgery; (3) PHS

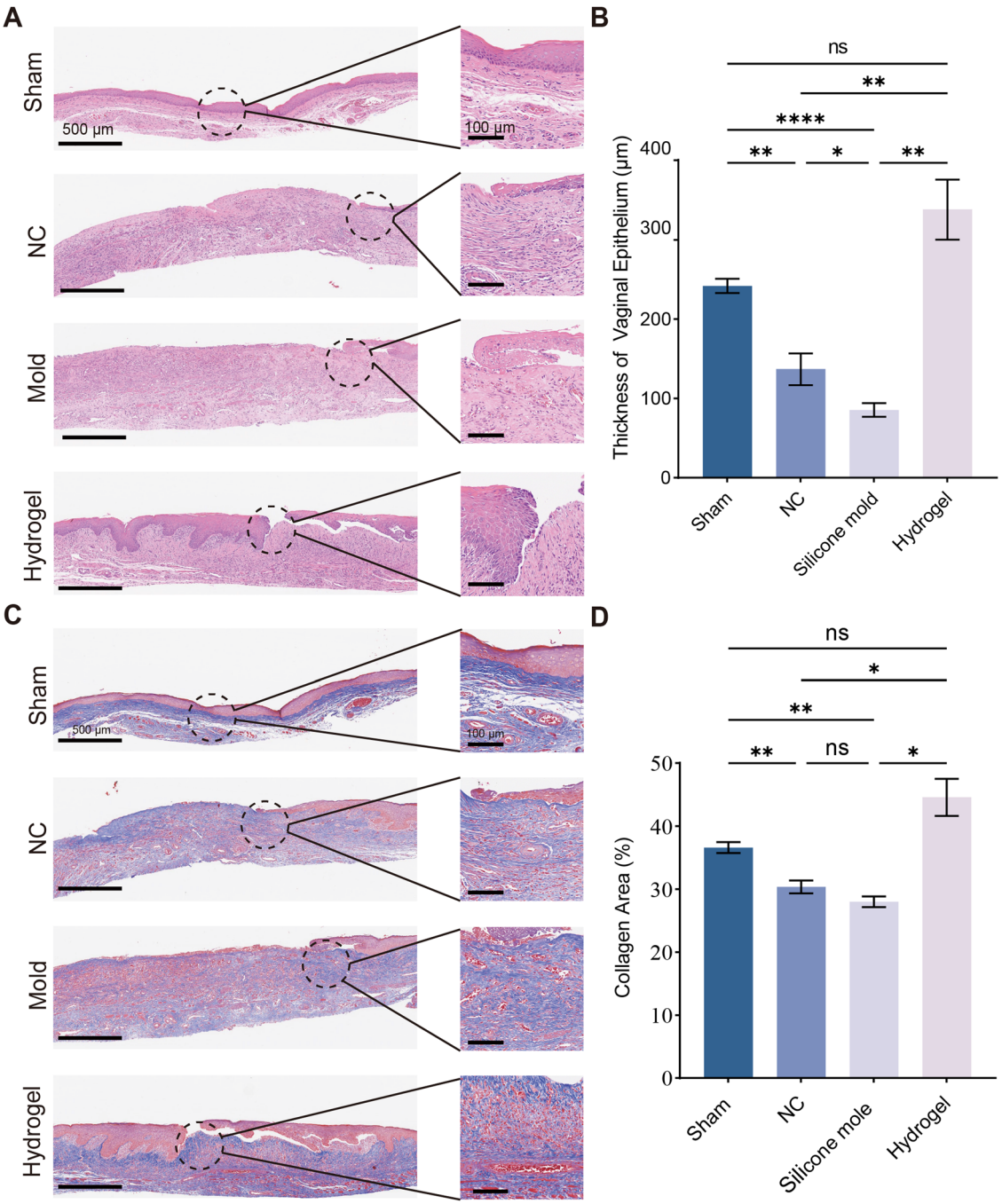

Fig. 6 Histological analysis of wound healing. (A) and (B) HE staining and quantitative analysis in the sham group, NC group, mold group, and PHS hydrogel group. (C) and (D) Masson staining and quantitative analysis in the sham group, NC group, mold group, and PHS hydrogel group. All data are reported as mean ± standard deviation. Significance levels are indicated as follows: * $p < 0.05$, ** $p < 0.01$, *** $p < 0.001$, and **** $p < 0.0001$. NS represents no significant difference.

hydrogel group, where PHS hydrogel was placed inside the vaginal cavity of model rats. We captured wound photos from days 1 to 5 to analyze the wound healing progress (Fig. 5A). The results indicated that the hydrogel group exhibited the best healing effect, with a wound closure rate of 95% on the 5th day, while the control group and mold group showed no statistically significant difference in wound closure rates, with only a 60% closure rate on the 5th day (Fig. 5B and C). The animal experiment results suggest that PHS hydrogel significantly promotes vaginal wound healing.

3.6 Histological analysis

To investigate the molecular mechanisms involved in the healing process of vaginal wounds, we employed a range of staining techniques including Hematoxylin and Eosin (H&E) staining, Masson's trichrome staining, Ki-67 immunohistochemical staining, and TGF-β immunohistochemical staining. In addition to the animal experimental groups used for vaginal wound assessment, we also prepared vaginal tissue sections from normal rats (without vaginal perforation surgery) as a sham group.

Through H&E staining, it was observed that the vaginal epithelium in the sham group was continuous, whereas in the negative control (NC) group, there were apparent defects in the vaginal epithelium, indicating successful model creation for rats with vaginal defects. Compared to the hydrogel group, the NC and mold groups exhibited discontinuity in the vaginal

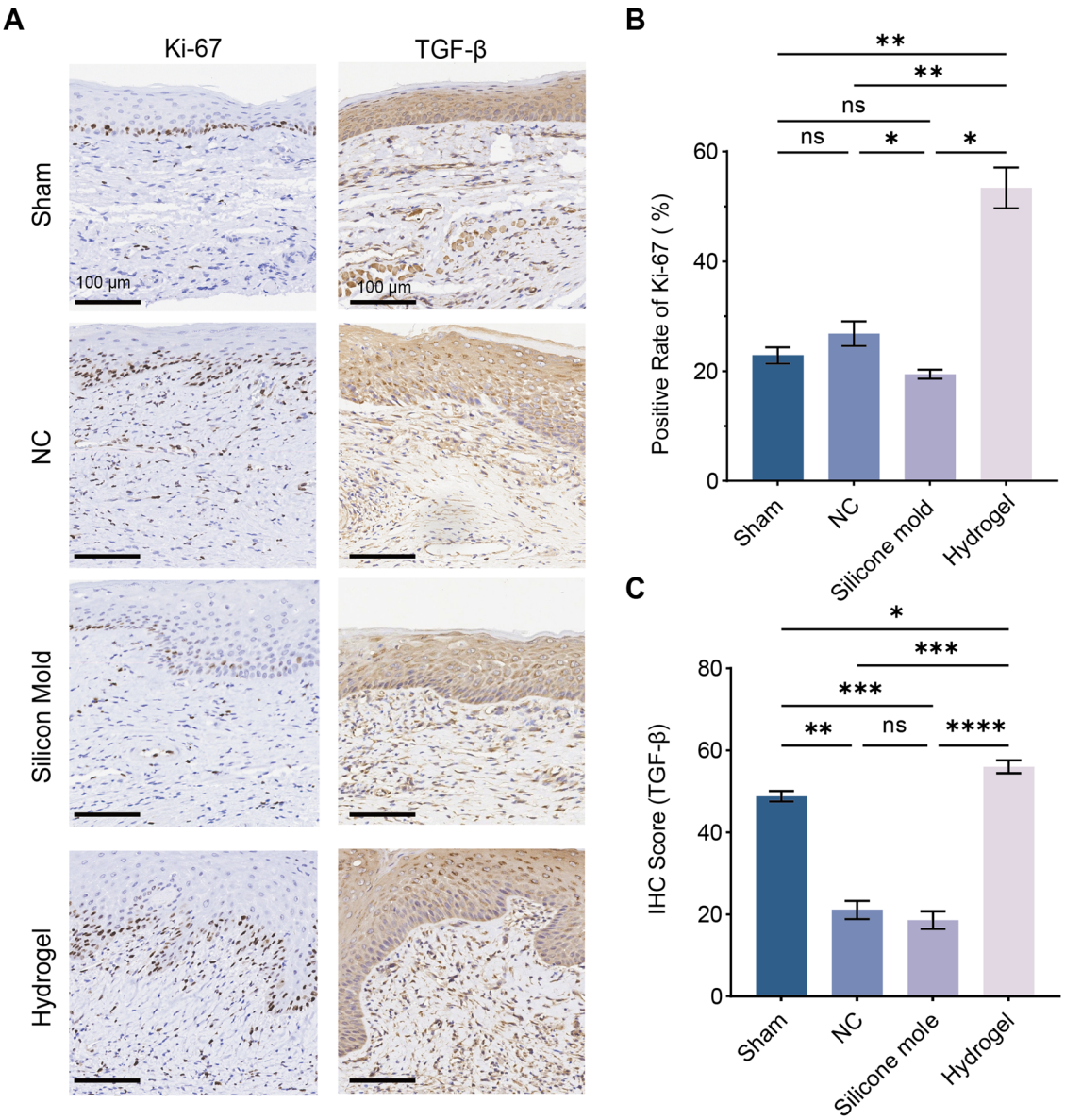

Fig. 7 Immunohistochemical staining of wound healing. (A) Ki-67 and TGF-β immunohistochemical staining in the sham group, NC group, mold group, and PHS hydrogel group. (B) Quantitative analysis of Ki-67 immunohistochemical staining. (C) Quantitative analysis of TGF-β immunohistochemical staining. All data are reported as mean ± standard deviation. Significance levels are indicated as follows: * $p < 0.05$, ** $p < 0.01$, *** $p < 0.001$, and **** $p < 0.0001$. NS represents no significant difference.

epithelium, and the regenerated epithelium was thinner than in normal vaginal epithelium. In the PHS hydrogel group, the defects were almost completely healed, and the epithelial layer was significantly thicker (Fig. 6A). In Masson's trichrome staining, positive areas indicate abundant collagen fibers. Among all groups, the PHS hydrogel group showed the most extensive positive areas (Fig. 6C). Ki-67, a marker for cell proliferation, indicates active cell division when positive cells are numerous. In Ki-67 immunohistochemical staining (Fig. 7A), the PHS hydrogel group had the highest number of Ki-67 positive cells. TGF-β, a cytokine, promotes cell proliferation and differentiation and plays a crucial role in tissue repair. Through TGF-β immunohistochemical staining (Fig. 7A), the PHS hydrogel group showed the highest positive area for TGF-β. Statistical results indicate that the hydrogel group had the highest vaginal epithelial thickness, collagen area proportion, Ki-67 positive cells, and TGF-β positive area proportion. These findings suggest that PHS hydrogel significantly promotes the growth of vaginal epithelium, and this promotive effect might be facilitated through enhanced collagen deposition and increased cell proliferation, thereby accelerating wound healing.

The vaginal epithelium plays a crucial role in the health of the reproductive system. An intact vaginal epithelium serves as a protective barrier and secretes lactic acid to maintain the vaginal pH balance. This acidic environment helps prevent the growth of harmful bacteria, thereby preserving vaginal health. When the vaginal epithelium is damaged, this barrier function is compromised, and the acidic environment in the vagina cannot be maintained. Vaginal epithelial regeneration is slow, which leads to prolonged healing of vaginal wounds. Therefore, promoting vaginal epithelial growth is a critical step in the treatment of vaginal wounds. The PHS hydrogel we developed accelerates the repair of the vaginal epithelium by enhancing the proliferation of vaginal epithelial cells and collagen deposition, thus expediting the restoration of the vaginal barrier and the maintenance of the acidic vaginal environment.

4 Conclusion

Herein, a kind of PHS hydrogel containing E2 is successfully prepared by constructing physical and chemical double network hybrid cross-linking. The hydrogel has a tight and strong network structure, and has good mechanical properties (tensile ratio at break is 109.2%, tensile strength is 176.52 kPa) and fatigue resistance. The compressive strength of the hydrogel after 1000 cycles of compression under 20% strain is almost unchanged, and the compressive strength of the hydrogel after 100 cycles of compression under 50% big strain only decreases by 5.29 kPa. At the same time, PHS hydrogel has excellent anti-swelling performance. After 60 days of swelling, the swelling ratio is only 2.92% higher than that of the first day, with excellent stability. In both *in vitro* and *in vivo* biocompatibility experiments, PHS hydrogel exhibited excellent biocompatibility and safety. In a standardized rat vaginal defect model, PHS hydrogel demonstrated outstanding therapeutic effects, leading to increased wound healing rates (60% *vs.* 95%). Histological staining and immunohistochemistry results indicated that PHS hydrogel accelerated wound healing by increasing collagen deposition and promoting cell proliferation. In combination with the above advantages, PHS hydrogel can not only be used as a support material for vaginal fixation, but also can release estrogen slowly and stably for a long time to promote cell proliferation and collagen fiber precipitation, and accelerate vaginal wound healing. As a ''fixed support-drug slowly release'' system, PHS hydrogel provides a new method for the treatment of vaginal defects.

Conflicts of interest

There are no conflicts to declare.

Acknowledgements

This study was supported by National Natural Science Foundation of China (No. 52203013); Sichuan Science and Technology Program (2024NSFSC1030); the Opening Project of State Key Laboratory of Polymer Materials Engineering (Sichuan University) (No. sklpme2022-4-09); 2021 Tianfuqingcheng Project (No. chuanqingcheng 903); Sichuan Provincial Medical Youth Innovation Research Project Plan (No. Q21009).

Notes and references

1 N. A. Okeahialam, A. H. Sultan and R. Thakar, *Am. J. Obstet. Gynecol.*, 2023, S991–S1004.
2 N. Callens, S. Weyers, S. Monstrey, S. Stockman, B. Van Hoorde, E. Van Hoecke, G. De Cuypere, P. Hoebeke and M. Cools, *Am. J. Obstet. Gynecol.*, 2014, **211**, 228.e1–e12.
3 S. A. Fish, *Am. J. Obstet. Gynecol.*, 1956, **72**, 544–548.
4 H. K. Haefner, H. F. Andersen and M. P. Johnson, *Obstet. Gynecol.*, 1991, **78**, 986–988.
5 N. Chen, S. Song, X. Bao and L. Zhu, *Front. Med.*, 2022, **16**, 859–872.
6 A. M. Raya-Rivera, D. Esquiliano, R. Fierro-Pastrana, E. López-Bayghen, P. Valencia, R. Ordorica-Flores, S. Soker, J. J. Yoo and A. Atala, *Lancet*, 2014, **384**, 329–336.
7 J. M. McCracken, S. Balaji, S. G. Keswani and J. C.-E. Hakim, *Adv. Wound Care*, 2021, **10**, 165–173.
8 J.-X. Ding, L.-M. Chen, X.-Y. Zhang, Y. Zhang and K.-Q. Hua, *Hum. Reprod.*, 2015, **30**, 581–589.
9 M. Kosiak, *Arch. Phys. Med. Rehabil.*, 1959, **40**, 62–69.
10 D. Gawlitta, W. Li, C. W. J. Oomens, F. P. T. Baaijens, D. L. Bader and C. V. C. Bouten, *Ann. Biomed. Eng.*, 2007, **35**, 273–284.
11 Z. Zhu, Y. Zhang, Y. Zhang, H. Zhang, W. Liu, N. Zhang, X. Zhang, G. Zhou, L. Wu, K. Hua and J. Ding, *Hum. Reprod.*, 2019, **34**, 248–260.
12 Y. Zhang, Z. Zhu, K. Hua, L. Yao, Y. Liu and J. Ding, *Am. J. Transl. Res.*, 2018, **10**, 3762–3772.

13 Y. Abramov, A. R. Webb, S. M. Botros, R. P. Goldberg, G. A. Ameer and P. K. Sand, *Fertil. Steril.*, 2011, **95**, 1467–1470.
14 C. M. Ripperda, P. A. Maldonado, J. F. Acevedo, P. W. Keller, Y. Akgul, J. M. Shelton and R. A. Word, *Menopause*, 2017, **24**, 838–849.
15 T. I. Montoya, P. A. Maldonado, J. F. Acevedo and R. A. Word, *Biol. Reprod.*, 2015, **43**, 1–9.
16 T. Zhou, Z. Yang, Y. Chen, Y. Chen, Z. Huang, B. You, Y. Peng and J. Chen, *Cell. Physiol. Biochem.*, 2016, **38**, 959–968.
17 R. J. Santen, *Climacteric*, 2015, **18**, 121–134.
18 C. M. Mitchell, J. C. Larson, C. J. Crandall, S. Bhasin, A. Z. LaCroix, K. E. Ensrud, K. A. Guthrie and S. D. Reed, *JAMA Network Open*, 2022, **5**, e2241743.
19 C. J. Crandall, K. M. Hovey, C. A. Andrews, R. T. Chlebowski, M. L. Stefanick, D. S. Lane, J. Shifren, C. Chen, A. M. Kaunitz, J. A. Cauley and J. E. Manson, *Menopause*, 2018, **25**, 11–20.
20 J. Li, L. Li, T. Wu, K. Shi, Z. Bei, M. Wang, B. Chu, K. Xu, M. Pan and Y. Li, *et al.*, *Small Methods*, 2023, 2300843.
21 Y. Fang, S. Huang, Q. Hu, J. Zhang, J. A. King, Y. Wang, Z. Wei, J. Lu, Z. He and X. Kong, *et al.*, *ACS Nano*, 2023, 24883–24900.
22 Y. Wang, P. Pan, H. Liang, J. Zhou, C. Guo and J. Wu, *Biomacromolecules*, 2020, **25**(2), 819–828.
23 J. Li, G. Wei, G. Liu, Y. Du, R. Zhang, A. Wang, B. Liu, W. Cui, P. Jia and Y. Xu, *Adv. Sci.*, 2023, **10**, 2207381.
24 X. Xie, X. Ao, R. Xu, H. lv, S. Tan, J. Wu, L. Zhao and Y. Wang, *Int. J. Biol. Macromol.*, 2024, 132363.
25 Y.-W. Kim, J. E. Kim, Y. Jung and J.-Y. Sun, *Mater. Sci. Eng., C*, 2019, **95**, 86–94.
26 J. Yang, V. Cristian, A. Dong and J. Zhang, *Macromol. Chem. Phys.*, 2021, **222**, 2000429.
27 J. Zhang, P. Peng, L. Chen, L. Zhao and J. Feng, *Polym. Test.*, 2021, **95**, 107087.
28 J.-Y. Sun, X. Zhao, W. R. Illeperuma, O. Chaudhuri, K. H. Oh, D. J. Mooney, J. J. Vlassak and Z. Suo, *Nature*, 2012, **489**, 133–136.
29 J. Li, W. R. Illeperuma, Z. Suo and J. J. Vlassak, *ACS Macro Lett.*, 2014, **3**, 520–523.
30 O. Gorke, M. Stuhlmüller, G. E. Tovar and A. Southan, *Mater. Adv.*, 2024, 2851–2859.
31 M. C. Darnell, J.-Y. Sun, M. Mehta, C. Johnson, P. R. Arany, Z. Suo and D. J. Mooney, *Biomaterials*, 2013, **34**, 8042–8048.
32 S. Bian, L. Hao, X. Qiu, J. Wu, H. Chang, G.-M. Kuang, S. Zhang, X. Hu, Y. Dai and Z. Zhou, *et al.*, *Adv. Funct. Mater.*, 2022, **32**, 2207741.
33 Z. Yuan, Z. Wan, Z. Tian, Y. Han, X. Huang, Y. Feng, W. Xie, X. Duan, S. Huang and X. Liu, *et al.*, *Chem. Eng. J.*, 2022, **450**, 138076.
34 Z. Wan, J. He, Y. Yang, T. Chong, J. Wang, B. Guo and L. Xue, *Acta Biomater.*, 2022, **152**, 157–170.
35 X. Xie, R. Xu, H. Ouyang, S. Tan, C. Guo, X. Luo, Y. Xie, D. Wu, X. Dong and J. Wu, *et al.*, *J. Mater. Chem. B*, 2022, **10**, 8684–8695.
36 L. Xin, X. Zheng, J. Chen, S. Hu, Y. Luo, Q. Ge, X. Jin, L. Ma and S. Zhang, *Adv. Healthcare Mater.*, 2022, **11**, 2201680.
37 W. Li, S. Wu, L. Ren, B. Feng, Z. Chen, Z. Li, B. Cheng and J. Xia, *ACS Nano*, 2023, **17**, 22106–22120.
38 X. Zou, X. Kui, R. Zhang, Y. Zhang, X. Wang, Q. Wu, T. Chen and P. Sun, *Macromolecules*, 2017, **50**, 9340–9352.
39 K. Cui, Y. N. Ye, T. L. Sun, C. Yu, X. Li, T. Kurokawa and J. P. Gong, *Macromolecules*, 2020, **53**, 5116–5126.
40 W. Cui, Y. Cai, Y. Zheng and R. Ran, *Polymer*, 2020, **210**, 123042.
41 T. L. Sun, T. Kurokawa, S. Kuroda, A. B. Ihsan, T. Akasaki, K. Sato, M. A. Haque, T. Nakajima and J. P. Gong, *Nat. Mater.*, 2013, **12**, 932–937.
42 S. Y. Zheng, H. Ding, J. Qian, J. Yin, Z. L. Wu, Y. Song and Q. Zheng, *Macromolecules*, 2016, **49**, 9637–9646.
43 L. A. Wallace, L. Gwynne and T. Jenkins, *Ther. Delivery*, 2019, **10**, 719–735.
44 E. V. Vodegel, A. W. Kastelein, C. H. Jansen, J. Limpens, S. E. Zwolsman, J.-P. W. Roovers, C. R. Hooijmans and Z. Guler, *Neurourol. Urodyn.*, 2022, **41**, 115–126.
45 M. Tian, J. Shuai, B. A. Bishop, W. Zhang, J. Chen and X. Wang, *Chem. Eng. J.*, 2023, **476**, 146751.
46 L. Qiao, Y. Liang, J. Chen, Y. Huang, S. A. Alsareii, A. M. Alamri, F. A. Harraz and B. Guo, *Bioact. Mater.*, 2023, **30**, 129–141.